Resonances and threshold phenomena in low-energy electron collisions with hydrogen halides: new experimental and theoretical results

M. Čížek, J. Horáček

Institute of Theoretical Physics, Faculty of Mathematics and Physics, Charles University Prague, V Holešovičkách 2, 180 00 Praha 8, Czech Republic

M. Allan

Institute of Physical Chemistry, University of Fribourg, Pérolles, CH-1700 Fribourg, Switzerland

W. Domcke

Institute of Physical and Theoretical Chemistry, Technical University of Munich, D-85747 Garching, Germany

Received 9 May 2002;
final version 12 August 2002

Low-energy electron collisions with HCl and HBr and the deuterated compounds have been investigated by experimental and theoretical methods. New experimental results have been obtained on relative differential cross-sections for vibrational excitation and dissociative electron attachment. Measurements with high energy resolution for rotationally cooled molecules have revealed, in addition to shape resonance, threshold peaks and Wigner cusps, the existence of surprisingly sharp oscillatory structures in the elastic and $v = 0 \rightarrow 1$ vibrational excitation cross-sections in a narrow range below the dissociative attachment threshold. The theoretical analysis is based on an improved nonlocal resonance model which has been constructed on the basis of ab initio fixed-nuclei scattering phase shifts for HCl and HBr and accurate ab initio calculations of the bound part of the HCl^- and HBr^- potential-energy functions. The high degree of agreement which has been obtained between experiment and theory for all channels indicates that the mechanisms responsible for the rich threshold structures in the collision cross-sections are completely understood.

PACS: 34.80.Ht
Key words: electron–molecule collisions, electron detachment, resonances, hydrogen halides

1 Introduction

About 25 years ago, the discovery of pronounced threshold peaks in the vibrational excitation (VE) cross-sections of HF, HCl and HBr by Rohr and Linder [1–3] has initiated extensive experimental and theoretical research on low-energy collisions of electrons with hydrogen halides. The experimental studies unveiled a multitude of interesting phenomena (cusps at threshold for VE in elastic [4] and inelastic [1–3] channels and step-like structures at VE thresholds in the cross-section

for dissociative attachment (DA) [5, 6] have been discovered at about the same time as the threshold peaks). Narrow interference structures in the $v = 0 \rightarrow 1$ and $v = 0 \rightarrow 2$ cross-section of HF have been observed by Knoth et al. [7] and assigned to vibrational Feshbach resonances. A series of detailed studies of angularly resolved rovibrational excitation cross-sections of HF and HCl has subsequently been performed by Ehrhardt and coworkers (Ref. [8] and references therein).

More recently, not only more accurate determinations of the shape and intensity of the threshold peaks and cups structures in the VE functions of hydrogen halides have become possible, but also additional unexpected phenomena have been discovered. Cvejanović and Jureta [9] and Cvejanović [10] reported narrow oscillatory structures in the $v = 0 \rightarrow 1$ and $v = 0 \rightarrow 2$ VE cross-sections of HCl. The existence of these oscillations has been confirmed by Schafer and Allan [11]. Very recently, these narrow oscillatory structures have been revealed with much better resolution in both HCl and HBr by applying rotational cooling of the target gas in a free jet expansion [12, 13]. New results have been obtained for HF by extension of the measurements up to the $v = 4$ channel, revealing the existence of oscillatory structures also in this system [14]. Completing the investigation of the hydrogen halide series, Sergenton et al. [15] have reported data on the VE cross-sections of HI up to $v = 8$. The measurements confirmed the theoretically expected [16] absence of threshold peaks and the existence of extended s-wave-type Wigner cusps structures [15].

The experimental research on low-energy electron scattering from hydrogen halides has been accompanied by intense theoretical efforts over many years. A variety of theoretical concepts and methods have been developed to explain the experimental findings, among them rovibrational close-coupling expansions [17], extensions of the R-matrix method to account for nuclear dynamics [18, 19], effective-range models [20] and the so-called nonlocal resonance model based on the Feshbach projection operator approach [21]. A complete survey of the theoretical developments can be found in reviews by Morrison [22], Fabrikant [23], Domcke [24] and Horáček [25].

In the present article we summarise the results of recent experimental [12, 13] and theoretical [13, 26] work on low-energy collisions of electrons with HCl and HBr. This work has lead to a remarkable degree of understanding of the pronounced resonance and threshold effects in the VE and DA cross-sections.

In view of the diversity of resonance and threshold phenomena in low-energy electron collisions with hydrogen halides mentioned above, it may be helpful to provide a brief explanation of the concepts and the terminology, to which we refer to in the following.

The expression "threshold peak" has been introduced by Rohr and Linder to describe a pronounced enhancement of a VE cross-section in a narrow energy range above the threshold for this process, as observed in HF, HCl and H_2O, for example [1–3]. Most threshold peaks known to date have been found in small polar molecules. The term is descriptive in nature; therefore it can be a matter of interpretation whether an enhancement of an inelastic cross-section at threshold should be called a threshold peak.

"Wigner cusps" are generic features of low-energy multi-channel scattering [27]. As a consequence of the unitarity of the S matrix, a steplike onset of the cross-section for a new channel must be accompanied by sharp variations of the cross-sections of the other open channels in the vicinity of the threshold. A threshold peak represents a particularly steep and intense onset of the cross-section and is therefore to be expected to be accompanied by unusually sharp and pronounced Wigner cusps.

"Vibrational Feshbach resonances" (also referred to as "nuclear excited Feshbach resonances" [28]) are quasi-bound vibrational energy levels associated with the potential-energy function of an electronically bound anion state. These levels are nonstationary because they can decay into the electronic continua of lower vibrational levels of the target molecule. Experimentally, vibrational Feshbach resonances have been particularly well characterised for the $e^- + HF$ system [7, 14]. Vibrational Feshbach resonances are generally expected to exist in polar molecules somewhat below target vibrational levels which are located below the DA threshold.

"Outer-well resonances" have been discovered recently as very narrow structures in elastic and VE cross sections of HCl and HBr [12, 13]. They represent vibrational energy levels in the shallow and wide outer well in the potential-energy functions of HCl^- and HBr^- at intermediate internuclear distances [12, 13]. The outer-well resonances are bound levels with respect to dissociation into $H+X^-$, but can decay, like vibrational Feshbach resonances, by electron emission into the open vibrational channels of HX.

The concept of "boomerang oscillations" has been introduced by Herzenberg to characterise oscillatory interference structures in the VE cross-sections of N_2 [29]. At that time, boomerang oscillations were considered as a characteristic signature of shape resonances (see [30] for the explanation of the terms "shape resonance" and "Feshbach resonance" in electron-molecule scattering) of intermediate width, i. e., $\Gamma \approx \omega$, where Γ is the decay width of the resonance and ω the vibrational frequency. More recently, boomerang-type oscillations also have been detected in VE cross-sections associated with very broad shape resonances such as the $^2\Sigma_u^+$ resonance in $e^- + H_2$ [31] and the $^2\Sigma$ resonance in $e^- + HCl$ [9, 12]. In these systems the boomerang oscillations appear as sharp and narrowly spaced oscillatory structures which converge towards the DA threshold from below [14].

2 Experimental methods

Measurements of threshold peaks in cross-sections with electron spectrometers utilising electrostatic lenses and energy selectors represent a substantial challenge to the experimentalist. Threshold peaks are easily missed because weak unwanted electric or magnetic fields in the collision region prevent very slow electrons from reaching the detector. On the other hand, these instruments may measure large signal peaks at threshold even in absence of true peaks in the cross-section, because slow electrons can be collected from large solid angles and this (nearly) total collec-

tion may occur even when it is not intended. A magnetically collimated spectrometer using trochoidal analysers is much less prone to these problems — it provides a more stable response function near threshold. We therefore used this instrument [32], which measures vibrationally inelastic cross-sections at 0° and 180°, to obtain a reliable indication of the shape of the threshold peaks. The high sensitivity of this instrument has permitted measurements up to the $v = 0 \rightarrow 6$ transition in HCl and HBr. The resolution of this instrument is around 50 meV in the energy-loss mode.

The superior resolution of a spectrometer with hemispherical electrostatic analysers [33] is used to reveal fine structure in the elastic and the $v = 0 \rightarrow 1$ cross-sections. The resolution used in the present studies has been around 20 meV in the energy-loss mode, corresponding to around 15 meV in the incident electron beam. The reliability of this instrument for measurements near threshold has recently been improved by adding an additional degree of freedom in compensating unwanted residual electric fields in the collision region. The visibility of the present structures, whose position depends on the rotational quantum number of the target molecule, has been further improved by rotationally cooling the target gas in a supersonic expansion. The electrostatic instrument has also been used to measure relative DA cross-sections. Fragment ions and scattered electrons were separated by a small Wien filter. More details on the experimental methods can be found in Refs. [12, 13].

3 Nonlocal resonance model

The nonlocal resonance model is based on the assumption that a temporary molecular negative-ion state (resonance) is formed and that this resonance accounts for the coupling of the electronic scattering dynamics with the nuclear motion [34]. The resonance is represented by a square-integrable discrete state $|\varphi_\mathrm{d}\rangle$ which interacts with a continuum of scattering states $|\varphi_\varepsilon\rangle$ via coupling matrix elements $V_{\mathrm{d}\varepsilon}$. $|\varphi_\mathrm{d}\rangle$ and $|\varphi_\varepsilon\rangle$ are assumed to be diabatic states, that is, their wave functions vary smoothly with the internuclear distance R. The second essential ingredient of the nonlocal resonance model for hydrogen halides is the explicit consideration of threshold effects induced by the long-range dipole potential. The dipole-induced nonanalyticities of the S matrix and related quantities at threshold enter through the threshold expansion of the energy-dependent width function

$$\Gamma(\varepsilon) = 2\pi |V_{\mathrm{d}\varepsilon}|^2 \tag{1}$$

and the associated level shift $\Delta(\varepsilon)$ [34].

The basic equation of the nonlocal resonance theory is the wave equation describing nuclear motion in the short-lived anion state [24, 35]

$$\begin{aligned}&[T_\mathrm{N} + V_\mathrm{d}(R) - E]\,\Psi_\mathrm{d}(R)\\ &+ \int \mathrm{d}\varepsilon \int \mathrm{d}R'\, V_{\mathrm{d}\varepsilon}(R) G_0(R, R'; E-\varepsilon) V^*_{\mathrm{d}\varepsilon}(R') \Psi_\mathrm{d}(R') = -V_{\mathrm{d}\varepsilon_\mathrm{i}}(R)\chi_{v_\mathrm{i}}(R)\end{aligned} \tag{2}$$

with

$$G_0(R, R'; E) = \langle R|(E - T_\mathrm{N} - V_0 + \mathrm{i}\epsilon)^{-1}|R'\rangle. \tag{3}$$

Here $V_0(R)$ and $V_\mathrm{d}(R)$ are the potential-energy functions of the target state and the discrete state, respectively. $\chi_{v_\mathrm{i}}(R)$ is the wave function of the initial vibrational state of the target molecule, ε_i is the energy of the incoming electron, and E is the total energy of the collision complex. G_0 is the Green's function for nuclear motion in the target state, T_N being the radial nuclear kinetic energy operator.

The second term on the left hand side of Eq. (2) plays the role of a complex, energy-dependent and nonlocal effective potential for the radial nuclear motion. It accounts for the decay of the electronic resonance state through the coupling with the electronic scattering continuum.

From the solution of Eq. (2), the integral cross-section for electron scattering from initial vibrational state v_i to final state v_f is obtained as [24]

$$\sigma_{v_\mathrm{f}v_\mathrm{i}}(E) = \frac{4\pi^3}{k_\mathrm{i}^2}|\langle\chi_{v_\mathrm{f}}|V^*_{\mathrm{d}\varepsilon_\mathrm{f}}|\Psi_\mathrm{d}\rangle|^2. \tag{4}$$

This expression includes only the resonant part of the scattering amplitude, which is dominant for inelastic processes and a background scattering amplitude is neglected. In principle, the background amplitude can be deduced from the electronic wave function $|\varphi_\varepsilon\rangle$. Note, however, that this wave function is not required for the calculation of the cross-section (4) and for the solution of Eq. (2) if the matrix element $V_{\mathrm{d}\varepsilon}$ is known. For the resonant part of the elastic cross-section Eq. (4) with $v_\mathrm{f} = v_\mathrm{i}$ can also be used, but the interference of the resonant amplitude with the background scattering amplitude has to be taken into account.

The cross-section for dissociative attachment of an electron of energy ε_i to a molecule in the vibrational state $|\chi_v\rangle$ given in [24] is

$$\sigma_\mathrm{DA}(E) = \frac{4\pi^3}{k_\mathrm{i}^2}|\langle\Psi_\mathrm{d}|V_{\mathrm{d}\varepsilon_\mathrm{i}}|\chi_{v_\mathrm{i}}\rangle|^2, \tag{5}$$

where Ψ_d is now the solution of Eq. (2) in which the right hand side is set to zero.

In practice, the nuclear wave function $\Psi_\mathrm{d}(R)$ is represented by a partial wave expansion with respect to rotational angular momentum and the Lippmann-Schwinger equation corresponding to the wave equation (2) is solved for the individual partial wave components [36, 26]. For this purpose, the very efficient Schwinger–Lanczos continued-fraction method [37] is employed. The efficiency of this method allows to calculate the cross-sections on a very fine mesh of collision energies. To allow for a detailed comparison between experiment and theory, the theoretical data have been averaged over the rotational population distribution of the target gas and convoluted with an experimental resolution function (see [13] for details).

In all our calculations we assumed an isotropic (with respect to the mutual orientation of the internuclear axis and the momentum of electron) coupling amplitude $V_{\mathrm{d}\varepsilon}(R)$. The calculation with this assumption yields isotropic differential cross-section for both VE and DA processes. We can thus compare the energy-dependence of the experimental differential cross-sections (see Section 2) directly with the integral cross-sections (4) and (5) respectively. The assumption that the inelastic scattering is predominantly isotropic is also supported by experiments. Rohr and

Linder [2] found no significant angular dependence of differential VE cross-section for HCl. The isotropy of the differential cross-section for HCl within ±20% has been confirmed also in more recent measurements of Ehrhardt and coworkers (see [8] and references therein) with the exception of the close vicinity of the threshold (0.5 eV for $0 \rightarrow 1$ and 0.8 eV for $0 \rightarrow 2$ VE cross-sections).

The nonlocal resonance model is characterised by the three functions $V_0(R)$, $V_\mathrm{d}(R)$, and $V_{\mathrm{d}\varepsilon}(R)$. The target potential-energy function $V_0(R)$ can be directly obtained by ab initio calculations or by fitting spectroscopic data. The functions $V_\mathrm{d}(R)$ and $V_{\mathrm{d}\varepsilon}(R)$ representing the HX^- resonance (at short internuclear distance) and the HX^- bound state (at intermediate and large internuclear distances) have been obtained by a joint fitting of the ab initio $^2\sum$ eigenphase sum [38, 39] and accurate ab initio calculations [13, 40] of the HX^- potential-energy function at intermediate internuclear distances. All parameters of the model are thus determined by ab initio calculations. Compared to earlier models for HCl [21] and HBr [41], the recently constructed models [13, 26] incorporate two essential improvements: (i) the R-dependence of the dipole-induced threshold exponent is taken into account and (ii) the long range part of the HCl^- and HBr^- potential-energy functions is carefully modelled on the basis of very accurate ab initio calculations [13, 40] and asymptotic expansions. Detailed descriptions of the nonlocal resonance models for HCl and HBr are given in [13, 26].

The potential-energy functions of target molecule and negative ion, which are very useful for a qualitative interpretation of the observed structures in the cross-sections (see below), are shown in Fig. 1 for both HCl/HCl^- and HBr/HBr^-, respectively, together with the ab initio data for the bound part of the anion

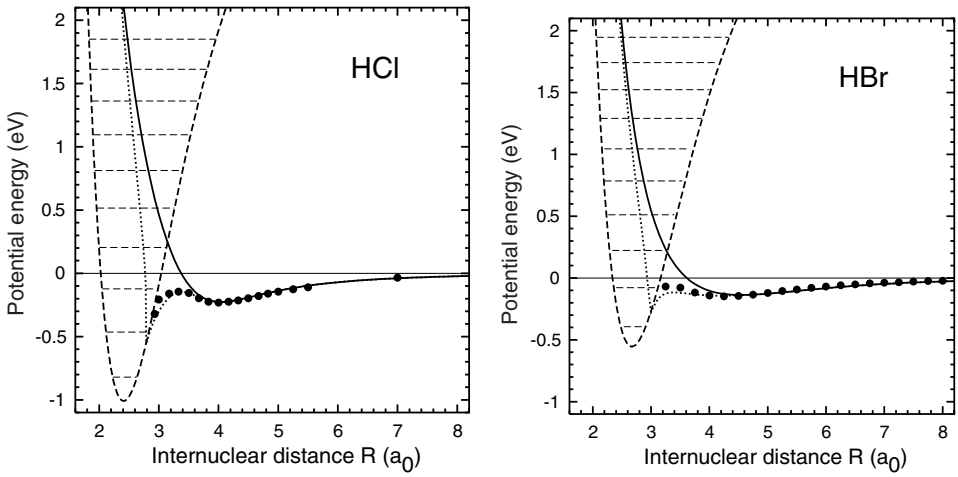

Fig. 1. Potential-energy functions for HCl and HBr. Dashed line: ground electronic state of the molecule with vibrational states indicated; solid line: discrete state potential $V_\mathrm{d}(R)$ of the molecular anion; dotted line: adiabatic potential curve within our model; dots: quantum-chemical data for the anions.

potential-energy functions. Noteworthy features are the sharp kink of the anion potential at the crossing with the target potential, caused by the stabilising effect of the dipole potential in the electron scattering channel, and the wide outer well in the HX^- potential function, supporting a number of quasibound vibrational levels which converge towards the dissociative attachment threshold.

4 Electron−HCl collisions

Vibrational excitation cross-sections for the transitions $v = 0 \to 1, v = 0 \to 2$ and $v = 0 \to 3$ obtained with the use of the nonlocal resonance model are shown in Fig. 2(left). These data should be compared with Fig. 2(right) showing the cross-sections measured with the magnetically collimated spectrometer. Very

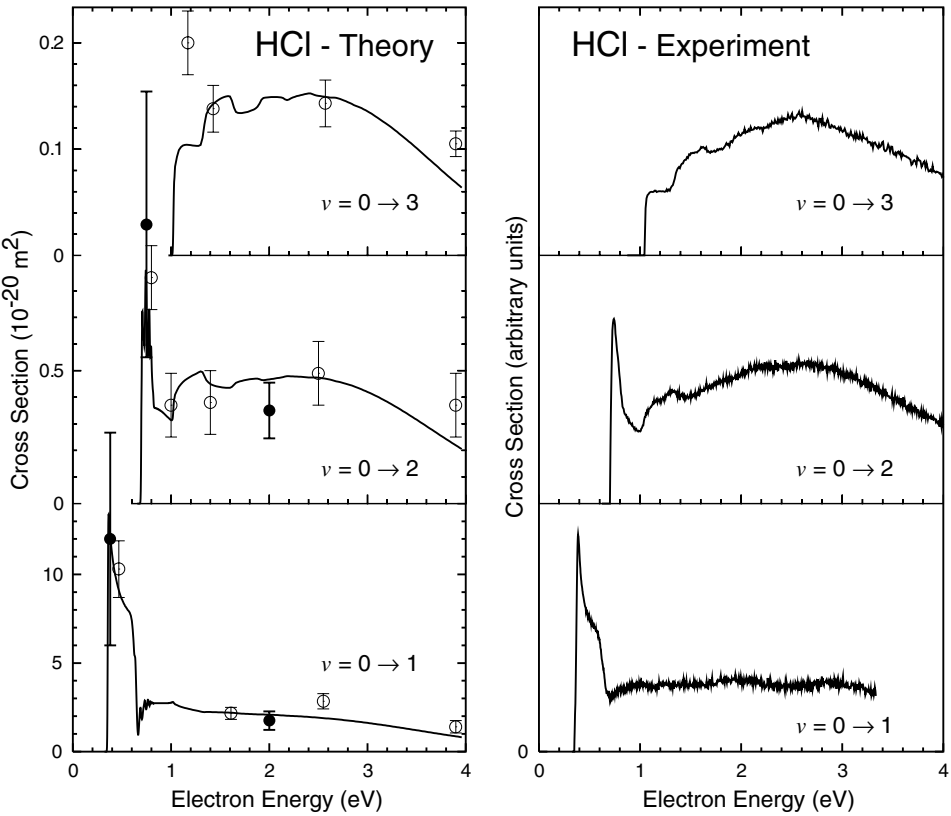

Fig. 2. Vibrational excitation in HCl. The theory (left) is compared to the experiment from the magnetically collimated instrument (right). The theoretical cross-sections are integrated over all angles, the experiment measures the sum of 0° and 180° differential cross-sections. Absolute values of the cross-section measured previously [2] and [8] (full and empty symbols, respectively) are included (left).

good agreement is found between theory and calculation. The shapes of the cross-sections in the threshold region are reproduced by the theory extremely well. The threshold peaks known to exist in the channels $v = 0 \rightarrow 1$ and $v = 0 \rightarrow 2$ and the cusps at openings of new vibrational channels are correctly reproduced. The calculated absolute values of the cross-sections are in good agreement with the absolute data reported by Rohr and Linder [2] for $v = 0 \rightarrow 1$ and $v = 0 \rightarrow 2$, if the latter are rescaled by a factor of 0.7 as suggested previously in the literature [38]. Our calculation is also in agreement with integral cross-sections of Ehrhardt and coworkers [8], with the exception of the threshold peak in $0 \rightarrow 3$ VE process which is confirmed neither by the calculation nor by the present measurement. We also would like to point out that although the absolute normalisation of the cross-section has not been measured in the present experiments, the relative heights of the curves on the right are based on the experimental ratios permitting comparison with the theory on the left in Fig. 2.

In the right hand part of Fig. 3 we compare the calculated vibrational $v = 0 \rightarrow 1$ cross-section in the region below the threshold for the dissociative attachment with the recent experimental data [12] obtained with the high resolution spectrometer using hemispherical electrostatic analysers. The theoretical curves in Fig. 3 are for an assumed electron spectrometer of unlimited resolution, while the actual resolution of the experiment is about 15 meV. The experimental data are further broadened because of the contribution of several rotational states of the target molecules (the exact temperature reached by the rotational cooling is not known, it is estimated

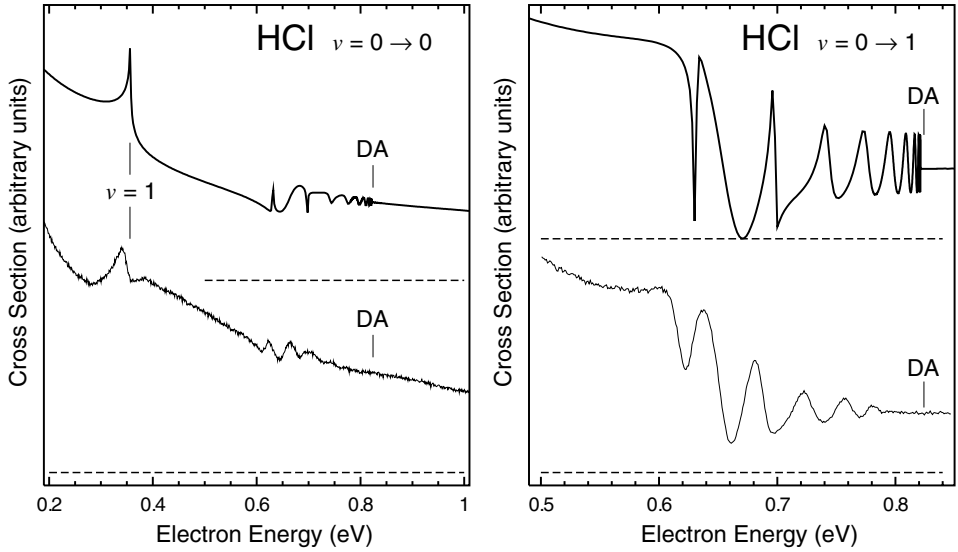

Fig. 3. Boomerang oscillations in the VE cross-sections for HCl. Top: theory, bottom: experiment (electrostatic instrument, differential cross-section at 90°). The thresholds for dissociative attachment and 0→1 vibrational excitation are indicated.

to be around 100 K). A series of oscillations converging to the DA threshold is observed, in good agreement with theory. The agreement can be improved taking into account the rotational broadening and experimental resolution in the calculation — see the next section. A closer analysis shows that two different types of resonances contribute to these structures [12]. The two narrow and somewhat irregular structures in the upper trace of the right hand part of Fig. 3 have been identified as outer-well resonances [12]. The remaining more regular structures are reminiscent of boomerang-type oscillations, known, for example, from shape resonances in N_2 and H_2 [30, 31]. The exact positions and phases of the oscillations are very sensitive to the details of the potential $V_d(R)$ — the good agreement of experiment and theory is thus a proof of high accuracy of the ab initio potential curve.

This agreement extends even to the case of elastic scattering. The differential elastic cross-section measured with the electrostatic instrument at 90° [12] is compared with the calculated resonant part of the integral elastic cross-section in the left part of Fig. 3. It also has to be recalled that the calculation with the nonlocal resonance model does not include the contribution of background scattering to the elastic scattering amplitude. As is well known, the experimental elastic cross-section is strongly forward peaked, as expected for a polar target, but the role of background scattering decreases with increasing scattering angle, justifying the present comparison. The difference in the shape of the Wigner cusp at the $v = 1$ threshold between theory and experiment is presumably a consequence of neglecting the background amplitude in the calculation.

The narrowing of the oscillatory boomerang-type structures as they approach the DA threshold from below can be easily understood in the potential-energy picture of Fig. 1. The radial nuclear wave functions of the high-lying quasi-stationary levels are mostly localised in the outer well of the HX^- potential function, thus having little overlap with the radial nuclear wave functions of the target molecule. The convergence of the oscillating structures towards the dissociation attachment energy D is in fact nicely reproduced by the semiclassical formula for bound states in a $-C_4/R^4$ polarisation potential [42] ($C_4 = 2.25$ for long range $X^- + H$ interaction). In an alternative picture, the narrow oscillatory features can be interpreted as arising from the interference of strongly overlapping resonances [43].

5 Electron−HBr collisions

The theoretical results for the VE cross-sections of HBr for the first three channels are compared with the experimental data in Fig. 4. Pronounced threshold peaks are found only in the $v = 0 \to 1$ channel, in good agreement with the experimental data. Indication of a threshold enhancement of the VE cross-section is also seen in the $v = 0 \to 2$ channel, but here the height of the threshold signal barely exceeds the signal intensity of the broad shape resonance.

The oscillatory structures of the cross-sections in the region below the threshold for DA are shown in Fig. 5. As in the case of the HCl molecule, we plot in the left part of the Fig. 5 the elastic scattering cross-sections and in the right part the cross-

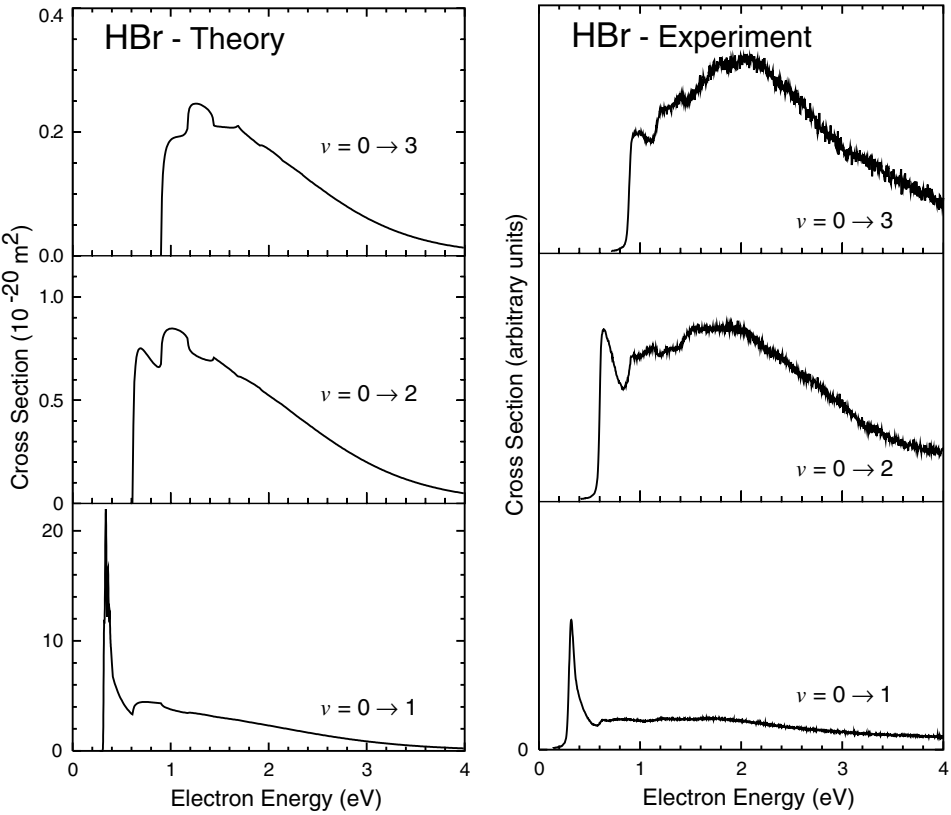

Fig. 4. Vibrational excitation of HBr. Theory versus experiment; experimental data have been obtained with the magnetically collimated instrument.

sections of $v = 0 \rightarrow 1$ excitation. The theoretical curves include an averaging over the population of rotational states of the target gas with an assumed temperature of 100 K and convolution of the data with a Gaussian of 5 meV FWHM to simulate in part the finite resolution of the spectrometer (the degree of structure-loss in this averaging can be judged by comparing Fig. 5 with Fig. 3 for HCl). The agreement between the calculated and the measured cross sections is very good, considering that we neglected the background scattering amplitude for the elastic process.

Finally we shall briefly discuss the process of dissociative attachment. Figure 6 compares the calculated and measured DA cross-sections, at the gas temperature of 310 K, for HBr (left) and DBr (right) [13]. Pronounced Wigner cusps (at vibrational excitation thresholds indicated as short lines in the figures) are seen both in the calculated as well as measured cross-sections in perfect agreement between the theory and the measurement. A secondary peak is observed in both HBr and DBr DA cross-sections to the left of the main peak. It is caused by DA to thermally vibrationally and rotationally excited molecules in the target gas. In the case of

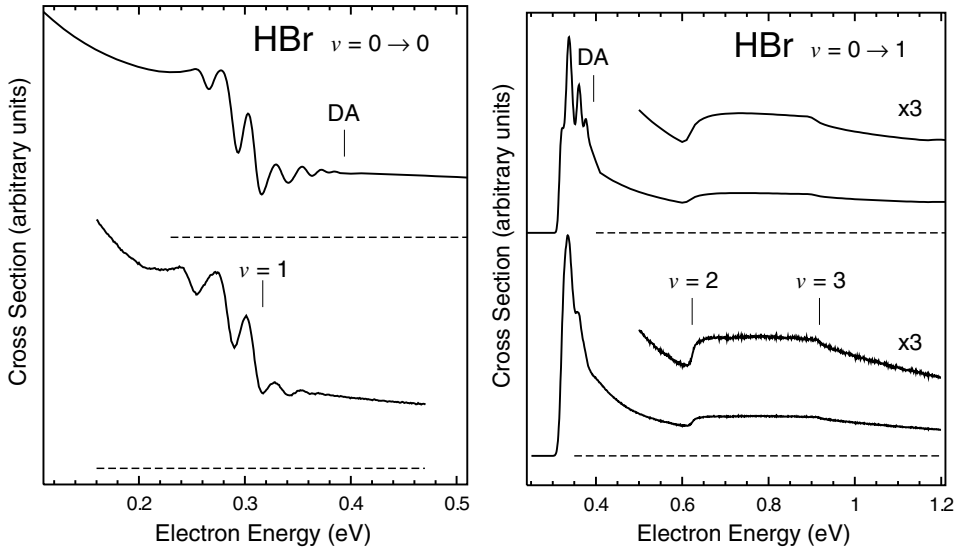

Fig. 5. The elastic (left) and VE (right) cross-sections for HBr. Top: theory (rotationally averaged for 100 K target gas temperature and convoluted with experimental resolution). Bottom: experiment (differential cross-section at 90° from the electrostatic instrument). The threshold energies for DA and VE processes are indicated.

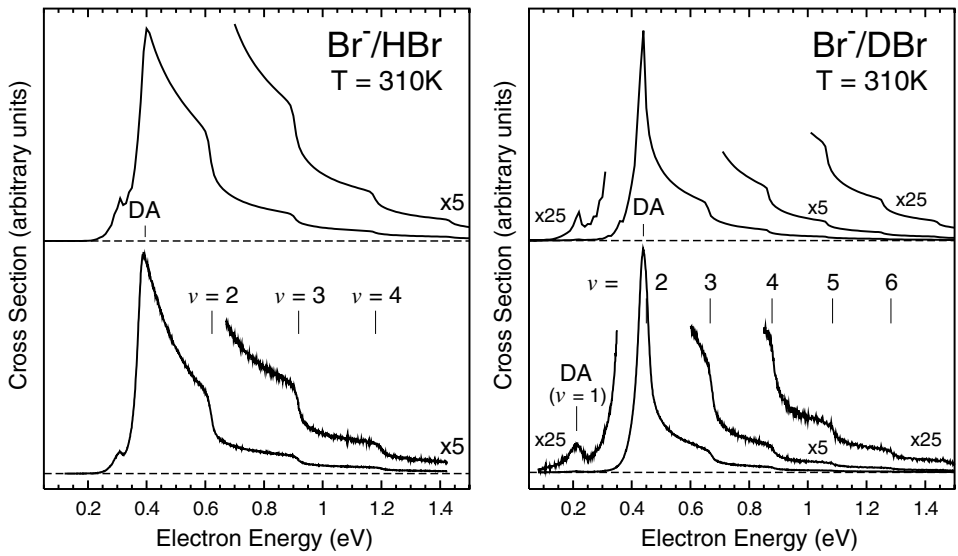

Fig. 6. DA cross-sections for HBr and DBr. The theory (top) versus experiment (bottom) for the gas temperature $T = 310$ K. The short lines and numbers (labeling final vibrational states) indicate the positions of Wigner cusps at the openings of vibrational excitation channels.

HBr mainly rotationally excited molecules (with $v = 0$) contribute, because near threshold the cross-section is enhanced by a Wigner cusp at the $v = 1$ VE threshold for molecules with angular momentum $J \approx 10$. On the other hand, the peak for DBr is caused by vibrationally excited molecules ($v = 1$ and J close to 0) in the target gas.

6 Conclusions

It is remarkable that the multitude of resonance and threshold phenomena in inelastic (VE) and reactive (DA) electron collisions with HCl and HBr can be quantitatively explained by a single (albeit energy-dependent and nonlocal) anion potential-energy function. The high degree of agreement between experiment and theory substantiates the nonlocal resonance model and confirms, moreover, the high quality of the underlying ab intio calculations, both static-exchange-polarisation electron-molecule scattering calculations [38, 39] as well as HX^- bound-state calculations [13, 40]. The development of a comparably detailed theoretical analysis for the e + HF and e + HI collision systems should be the subject of future work.

The recent completion of the experimental investigation of VE of hydrogen halides [12, 15] has definitively established that there exists a correlation between intense threshold peaks and the position of the final vibrational level relative to the DA threshold. Pronounced threshold peaks are only observed in hydrogen halides when the final vibrational level is located below or very close to the DA threshold ($v = 2$ in DBr is an example for the latter case [13]). This finding confirms previous theoretical interpretations [24, 28] which associate threshold peaks with vibrational Feshbach resonances, that is, quasi-bound levels of the anion which are located below the vibrational levels of the target molecule.

The boomerang-type oscillations and outer-well resonances which become visible in high-resolution electron-scattering measurement on rotationally cooled HCl and HBr molecules represent a very sensitive probe of the anion potential-energy function at intermediate and large internuclear distances. High-resolution low-energy electron scattering thus can provide information of spectroscopic quality on anion potential-energy surfaces which is not otherwise accessible. In the hydrogen halides it is the interplay of the dipole-induced enhancement of cross-sections at threshold, the low threshold for DA and the low value of the effective mass which renders this type of spectroscopy possible.

The theoretical models, which we used here for electron-HCl and electron-HBr collisions also predict cross-sections for the associative detachment process

$$X^- + H \rightarrow HX + e^- \qquad (X = Cl, Br). \tag{6}$$

The theory yields, in particular, detailed predictions for the energy spectrum of the detached electrons as a function of the ion-atom collision energy. These predictions are reported elsewhere [44].

This research was sponsored by Grant Agency of the Czech Republic, No. 203/00/1025, by Kontakt ME273 of Ministry of Education, Youth, and Physical Training of the Czech Republic and by project No. 2000-061543.00/1 of the Swiss National Science Foundation.

References

[1] K. Rohr and F. Linder: J. Phys. B **8** (1975) L200.

[2] K. Rohr and F. Linder: J. Phys. B **9** (1976) 2521.

[3] K. Rohr and F. Linder: J. Phys. B **11** (1978) 1849.

[4] P. D. Burrow: J. Phys. B **7** (1974) L385.

[5] R. Abouaf and D. Teillet-Billy: J. Phys. B **10** (1977) 2261.

[6] R. Abouaf and D. Teillet-Billy: Chem. Phys. Lett. **73** (1980) 106.

[7] G. Knoth, M. Gote, M. Rädle, K. Jung, and H. Ehrhardt: Phys. Rev. Lett. **62** (1989) 1735.

[8] H. Ehrhardt: in *Aspects of Electron-Molecule Scattering and Photoionization* (Ed. A. Herzenberg), American Institute of Physics, New York, AIP Conf. Proc. **204** (1989) 145.

[9] S. Cvejanović and J. Jureta: in *3rd European Conference on Atomic and Molec. Phys.*, Bordeaux 1989, Abstracts (unpublished), p. 638.

[10] S. Cvejanović: in *The Physics of Electronic and Atomic Collisions* (Eds. T. Andersen, B. Fastrup, F. Folkmann, H. Knudsen, and N. Anderson) (18th ICPEAC, Aarhus), American Institute of Physics, New York, AIP Conf. Proc. **295** (1993) 390.

[11] A. Schafer and M. Allan: J. Phys. B **24** (1991) 3069.

[12] M. Allan, M. Čížek, J. Horáček, and W. Domcke: J. Phys. B **33** (2000) L209.

[13] M. Čížek, J. Horáček, A. -Ch. Sergenton, D.B. Popović, M. Allan, W. Domcke, T. Leininger, and F.X. Gadea: Phys. Rev. A **63** (2001) 062710.

[14] A.-Ch. Sergenton, L. Jungo, and M. Allan: Phys. Rev. **A61** (2000) 062702.

[15] A.-Ch. Sergenton and M. Allan: Chem. Phys. Lett. **319** (2000) 179.

[16] J. Horáček, W. Domcke, and H. Nakamura: Z. Phys. D **42** (1997) 181.

[17] H.T. Thümmel, R.K. Nesbet, and S.D. Peyerimhoff: J. Phys. B **26** (1993) 1233.

[18] L.A. Morgan, P.G. Burke, and C.Z. Gillan: J. Phys. B **23** (1990) 99.

[19] I.I. Fabrikant, S.A. Kalin, and A.K. Kazansky: J. Phys. B **25** (1992) 2885.

[20] D. Teillet-Billy and J.P. Gauyacq: J. Phys. B **17** (1984) 4041.

[21] W. Domcke and C. Mündel: J. Phys. B **18** (1985) 4491.

[22] M.A. Morrison: Adv. At. Mol. Phys. **24** (1988) 51.

[23] I.I. Fabrikant: Commun. At. Mol. Phys. **24** (1990) 37.

[24] W. Domcke: Phys. Rep. **208** (1991) 97.

[25] J. Horáček: in *The Physics of Electronic and Atomic Collisions*, XXI ICPEAC, Sendai (Eds. Y. Itikawa et al.), American Institute of Physics, New York, 1999, p. 329.

[26] M. Čížek, J. Horáček, and W. Domcke: Phys. Rev. A **60** (1999) 2873.

[27] R.G. Newton: *Scattering Theory of Waves and Particles*, McGraw-Hill, New York, 1966, §17.2.

[28] J.-P. Gauyacq and A. Herzenberg: Phys. Rev. A **24** (1982) 2959.

[29] A. Herzenberg: J. Phys. B **1** (1968) 548.

[30] G.J. Schulz: Rev. Mod. Phys. **45** (1973) 423.

[31] M. Allan: J. Phys. B **18** (1985) L451.

[32] M. Allan: Helv. Chim. Acta **65** (1982) 2008.

[33] M. Allan: J. Phys. B **25** (1992) 1559.

[34] W. Domcke and L.J. Cederbaum: J. Phys. B **14** (1980) 149.

[35] J.N. Bardsley: J. Phys. B **1** (1968) 349.

[36] R.J. Bieniek: Phys. Rev. A **18** (1978) 392.

[37] H.-D. Meyer, J. Horáček, and L.S. Cederbaum: Phys. Rev. A **43** (1991) 3587.

[38] N.T. Padial and D.W. Norcross: Phys. Rev. A **29** (1984) 1590.

[39] R. Fandreyer, P.G. Burke, L.A. Morgan, and C.J. Gillan: J. Phys. B **26** (1993) 3625.

[40] P. Åstrand and G. Karlström: Chem. Phys. Lett. **175** (1990) 624.

[41] J. Horáček and W. Domcke: Phys. Rev. A **53** (1996) 2262.

[42] R.J. Leroy and R.B. Bernstein: J. Chem. Phys. **52** (1970) 3869; Chem. Phys. Lett. **5** (1970) 42.

[43] E. Narevicius and N. Moiseyev: Phys. Rev. Lett. **81** (1998) 2221.

[44] M. Čížek, J. Horáček, F.A.U. Thiel, and H. Hotop: J. Phys. B **34** (2001) 983.